Check for updates

Lethal weapon IL: a nano-copper/tetraalkylphosphonium ionic liquid composite material with potent antibacterial activity†

Abhinandan Banerjee, [ID] *[a] Bukola R. Aremu,‡[a] Sima Dehghandokht,‡[a] Rayan Salama,[a] Hao Zhou, [ID] [b] Sharon M. Lackie,[c] Moutasem Seifi,[a] Pierre Kennepohl [ID] [b] and John F. Trant [ID] *[ade]

Ionic liquid (IL) based composite materials have shown great promise as antimicrobial agents, owing to their inherent germicidal properties, as well as their ability to stabilize metal nanoparticles (NPs), which may serve as a secondary antimicrobial reservoir. Here, we show that tetraalkylphosphonium ILs (TAPILs) on their own can annihilate pathogens by interfering with their cell membranes; however, the nature of the alkyl substituents on the central P atom and the nature of the anion play decisive roles in determining their antimicrobial activities. Concomitantly, TAPILs can stabilize copper nanoparticles (Cu NPs) generated directly within the IL matrices without the addition of any secondary stabilizers. The composites thus generated were thoroughly characterized and shown to be far more lethal to *E. coli* than just the TAPILs alone. The antibacterial effect demonstrated by the composite, **composite-2**, created from P[6,6,6,8]Cl (**TAPIL-2**) was orders of magnitude more lethal to microbes in comparison with P[6,6,6,8]Cl or copper nanoparticles alone. Neither the parent **TAPIL-2** nor **composite-2** were compromised by ambient storage conditions over a period of months with regards to their bactericidal effects. **Composite-2** also proved to be effective against a panel of selected microbes. SEM studies were conducted to image *E. coli* after exposure to the TAPILs or **composite-2**; with the latter, only bacterial debris were noticed post-exposure, indicating total bacterial annihilation. The kinetic killing assay and regression analyses for time-dependent bactericidal activity of **composite-2** against *E. coli* and *S. aureus* demonstrated increase in log reduction values over time, indicating the effectiveness of **composite-2** in reducing the viable cell counts for both bacterial strains. Finally, Cu K-edge XANES was used to investigate the fate of Cu NPs within the composites, revealing oxidative disintegration of the Cu NPs within the TAPIL matrices over time. Copper ions and/or small copper clusters were released which interfere with the integrity and the permeability of *E. coli* cell membranes, inducing cell death. This was confirmed by SEM of bacterial preparations before and after exposure to both the TAPILs themselves as well as to the composites. Exposing *E. coli* to **composite-2** causes complete cellular destruction, leaving behind cellular debris as the only visible organic matter. Thus, these TAPIL-based composites containing 'ion reservoir' metal NPs are potent antimicrobial materials, deserving additional research.

[a]*Department of Chemistry and Biochemistry, University of Windsor, 401 Sunset Avenue, Windsor, Ontario N9B 3P4, Canada. E-mail: j.trant@uwindsor.ca; arb@uwindsor.ca*

[b]*Department of Chemistry, University of Calgary, 2500 University Drive NW, Calgary, Alberta, Canada, T2N 1N4*

[c]*Great Lakes Institute for Environmental Research (GLIER), University of Windsor, 2990 Riverside Drive, Windsor, Ontario N9B 3P4, Canada*

[d]*WeSpark Health Institute, 401 Sunset Avenue, Windsor, Ontario, N9B 3P4, Canada*

[e]*Binary Star Research Services, LaSalle, Ontario N9J 3X8, Canada*

† Electronic supplementary information (ESI) available: Additional NMR spectra of the TAPILs, a photographic representation of the change in copper speciation within **composite-2** over time, Fig. 8 plotted using logarithmic scales, and Table S1 showing the raw data for the time kill assay plots. See DOI: https://doi.org/10.1039/d3su00203a

‡ These two authors contributed equally.

Sustainability spotlight

The need for new effective sanitizers, especially those highly effective, easy to transport, and dilutable at point-of-use, has been highlighted by our renewed acquaintance with infectious diseases. The COVID-19 pandemic likewise highlighted the waste that is produced when a modern industrial economy faces a new threat. Extremely potent antimicrobial agents have promise for cleaning water and enhancing sanitation (SDG6), and reducing waste and fostering responsible production (SDG12), two of the UN Sustainable Development Goals. Both agents – quaternized phosphoniums and copper nanoparticles – are known to be effective antimicrobials on their own, but the effects are limited compared to a composite. Togehter they provide a material more than 2000-fold more effective than bleach, promising a safer, lower waste future.

1. Introduction

We are forever pursued by *Pestilence*, the First Horseman of the Apocalypse,[1] but the development and widespread deployment of antibiotics from the early 20th century certainly forced the horse to stumble and falter.[2] The respite, however, was transitory, and while we humans—as we tend to do—became complacent and lowered our guard,[3] the pale horse has clearly regained its footing to resume the chase. SARS-CoV-2,[4] the monkeypox virus,[5] and multi-drug resistant bacteria (such as *C. difficile*, *M. tuberculosis*, and *P. aeruginosa*)[6,7] are some examples of emergent pathogens, or concerning gain-of-function variations of existing pathogens, that are challenging the long period (at least in the developed world) of freedom from the scourge of infectious disease. These threats are either largely untreatable due to a lack of effective therapeutics, or are developing resistance to our dwindling supply of reserve antibiotics; to a greater or lesser extent, the post-antibiotic world has arrived.[8–10] Preventative engineering controls are required to contain their spread, including robust disinfection protocols.[11–13] The survival time of various bacteria on dry surfaces, for instance, can vary from a few days (*V. cholerae*, *B. pertussis*, and others) to a few months (*E. coli*, *S. aureus* including MSRA, and others).[14,15] The disinfection of commonly touched surfaces such as elevator buttons, staircase railing handles, keypads, and doorknobs, is of vital importance to prevent fomite transfer.[16] An alternative to continual disinfection by the application of, say, bleach—which is inconvenient, can damage a surface, and potentially needs either dedicated personnel or automation—would be the application of a benign coating with demonstrated antimicrobial properties onto these surfaces.[17,18] Some attempts have been made to infuse metallic door handles with copper (which is known to have antimicrobial properties),[19–21] but ideally, a coating that is easily applied to existing permanent fixtures *in situ* without having to take them apart would go a long way towards decreasing fomite-derived infection. As a first step towards this goal, the active components of this potential solution must be identified.

This need for sanitation is going to conflict directly with the need for sustainable solutions. Sanitizers are often quite concentrated, energy intensive to prepare, and can lead to pollution because of the large amounts used: consider, for instance, the concerns around quaternized ammonia[22] or bleach.[23] We need new solutions to address the joint challenges of emerging pathogens and environmental damage.

Tetraalkylphosphonium ionic liquids (TAPILs) are a class of poorly packed salts containing $[PR_4]^+$ (R = alkyl chains) cations and an inorganic or organic anion.[24] They exist as liquids at, or slightly above, ambient temperatures.[25] While other classes of ILs (such as alkylimidazolium ILs)[26] have been studied extensively in the last few decades for their antimicrobial properties, TAPILs themselves have not been explored as thoroughly in this context,[27,28] and those that have been have been quite short.[27,29,30] This lack of attention is unexpected: as ionic liquids they feature prominently in work relating to sustainable chemistry, and classical phosphonium salts are well established

antimicrobials.[31–33] TAPILS can stabilize suspended metal nanoparticles (NPs) without the need for secondary stabilizers.[34–36] They have also shown interesting properties related to catalyst recycling *vis-à-vis* the regeneration of catalytically deactivated metal NPs through redox cycles.[37–39]

In 2005, Seddon *et al.* examined the antibacterial action of a variety of TAPILs with the general formula $[PR_3R']X$, where R and R′ are alkyl groups and X is an anion such as halide, or a typical large non-coordinating ion.[40] They found that TAPILs with halide counterions, bearing alkyl chains ranging from pentyl to tetradecyl, showed antimicrobial activities particularly against cocci. This activity was found to be comparable to that of a standard commercial biocide—benzalkonium chloride. However, the exchange of the halide for other anions resulted in the loss of anti-microbial activity. In their search for a highly effective mitochondrial uncoupler based on TAPILs, Terekhova *et al.* synthesized a series of trialkyl phosphonium derivatives with varying alkyl chain lengths; the fourth substituent on the central P incorporated a *p*-chlorophenol entity separated by a spacer.[41] Of this series, the tripentylphosphonium-containing compound exhibited the most pronounced uncoupling activity in isolated rat liver mitochondria and an antibacterial effect on *B. subtilis*. Recently, Ermolaev and colleagues studied the antimicrobial activity of sterically hindered TAPILs. They found that tri-*tert*-butyl(*n*-dodecyl)phosphonium and tri-*tert*-butyl(*n*-tridecyl)phosphonium bromides demonstrated low cytotoxicity against normal human cells, but high antimicrobial activity against bacteria, including methicillin-resistant strains of *S. aureus* (MRSA).[42] Similarly, Mukherjee *et al.* examined the effect of two TAPILs [(tri-iso-butyl(methyl)phosphonium tosylate and trihexyl(tetradecyl)phosphonium bis-2,4,4-(trimethylpentyl) phosphinate)] against two bacterial strains [*B. subtilis* (Gram positive) and *E. coli* (Gram negative)] by measuring the diameter of the inhibition zone ("diz"); both the ILs exhibited greater antimicrobial activity than that of the commercial surfactant Triton-X-100.[43] Diphosphonium ILs such as 1,19-(1,10-decanediyl)bis(phosphonium[1,1,1-trihexyl]) chloride were synthesized by O'Toole *et al.*, and were found to be potent weapons against important eye pathogens, such as *S. aureus* (including MRSA strains), *P. aeruginosa*, and ocular fungal isolates, but benign to corneal epithelial cells in contrast to their monomeric analogues, which showed corneal cytotoxicity.[44] In 2021, Das *et al.* designed and synthesized monomeric and dimeric tri(hexyl)tetradecylphosponium fluoresceinate, and demonstrated that despite the absence of any significant anti-bacterial activity in sodium fluoresceinate, the corresponding TAPILs bearing $[HFl]^-$ and $[Fl]^{2-}$ anions were nearly twice as toxic to *E. coli* and over 10 times as toxic against *S. aureus* respectively in comparison with the chloride-bearing IL.[45] Through computational studies, they suggested that a multi-staged cell death mechanism involving cell growth inhibition through TAPIL-cell wall interactions and inhibition of RNA synthesis in bacterial cells together lead to bacterial cell death of bacteria exposed to fluoresceinate TAPILs. In 2022, Tetko and colleagues examined six alkyl triphenylphosphonium and alkyl tributylphosphonium bromides with C_8, C_{10}, and C_{12} alkyl chains, and found them to be promising lead structures

capable of annihilating drug-resistant *A. baumannii*.[46] There are some excellent reviews on the antimicrobial properties of other classes of ILs,[47,48] and the interested reader is referred to those for additional discussion.

A concern about any ionic organic agent is environmental persistence and toxicity. Medium chain TAPILs are toxic to zebrafish at concentrations around 100 mg L^{-1}, and long chain TAPILs at concentrations as low as 1 mg L^{-1}.[49] Similarly, ionic liquids more generally (although phosphoniums are understudied) are toxic to crustaceans at concentrations between 0.01 and 100 mg L^{-1} depending on the report.[50] Phosphonium ionic liquids also have a longer lifetime in the environment than other similar materials; however, they do degrade slowly over time,[51] although field tests have not been conducted. This all indicates that two criteria must be met for these materials to be used in any open system: they require extremely high efficacy so that they can be deployed at high dilution, ideally well below 1 mg L^{-1} at their useful concentration; and they must be field tested and examined for degradability before they can be manufactured. A further challenge for TAPILs is that, despite their promise, they are far more expensive than bleach. To be commercially relevant, they would need to be effective at a far lower concentration than observed in any of these studies. This could be possible through synergy with another antimicrobial agent. New solutions are required.

To the best of our knowledge, none of the studies to date incorporated a second germicidal entity within the TAPIL matrices to enhance activity; this is surprising, since the intrinsic NP-stabilizing nature of TAPILs is well-documented,[34,36,52,53] and Cu[54] and Ag NPs[55] have each been used as antimicrobial materials with some success. Recently, Clifford and colleagues reported the engineering of a nanocomposite coating containing Cu NPs with enhanced antibacterial properties.[56] In this report we examined three TAPILs (Fig. 1) with varying anti-bacterial effects. We correlated their bactericidal properties with their chemical structures. Then, we synthesized copper nanoparticles directly within these TAPILs, and tested the resulting composites against *E. coli* and *S. aureus* as representative Gram negative and positive bacteria, characterized the materials more completely, both in terms of physical and biological properties, and temporal stability, and evaluated them against a wide panel of bacteria. The materials show unprecedented promise and activity at extremely low concentrations and could form the basis of an effective alternative antiseptic.

We then determined that a 5-week storage did not diminish the antibacterial effects of our composites – *au contraire*, MIC and MBC values reduced over time, indicating the time-delayed release of a potent antibacterial agent. Using Cu K-edge XANES,

we determined that TAPILs in ambient atmosphere facilitate the release of copper ions and/or clusters from Cu NPs, which interfere with the structure and function of the bacterial cell membranes, causing cell lysis, as seen through SEM. A bacterial panel test revealed this to be the case not only for *E. coli* but for a variety of other bacteria, including multi-drug resistant *P. aeruginosa*. The progressive reduction in viable cell counts of *E. coli* and *S. aureus* upon exposure to **composite-2** indicates its effectiveness inhibiting bacterial growth over time. Given the minute amounts of composites needed for the elimination of bacteria, this approach can potentially be considered a sustainable antimicrobial solution.

2. Results and discussion

2.1. Preparation of the TAPILs and synthesis of the Cu/TAPIL composites

Although any TAPIL can be readily generated from the corresponding trialkyl phosphine, or from lower order phosphines with the appropriate equipment, or even from phosphine gas with appropriate precautions,[31] the commercial availability of a series of TAPILs makes this unnecessary for a preliminary study. The three TAPILs used in this study (Fig. 1), were purchased from Strem Chemicals, were dried in a vacuum oven (60 °C for 6–8 hours), and their purity confirmed by ^{1}H and ^{31}P NMR to rule out the presence of phosphorous or proton-containing impurities (Fig. S1–S3†). All TAPILs are built on a trihexylphosphine base; these alkyl chains are inherently longer than those that have tended to be previously explored by others. They vary by the nature of the fourth group or the nature of the complexing ion. **TAPIL-1** was the chloride salt of the "long" C-14 chain; **TAPIL-2** the chloride salt of the "short" C-8 chain; and **TAPIL-3** the triflimide of the "long" C-14. The chloride ions are hard, nucleophilic, and as coordinating as they can be, considering the nature of the cation. The triflimide is a poorly coordinating ion for comparison and should result in better charge separation in solution.

These TAPILs were then used as the medium for the synthesis of the Cu NPs. CuCl was converted to Cu NPs using LiAlH$_4$. The resulting TAPILs thus contain both Cu NPs and aluminum and lithium chloride salts (see Materials and methods for additional detail). The resulting composites could be stored in the fridge (4 °C) under nitrogen until needed for further studies. The composites remain stable when open to the atmosphere, although we do note slow changes in the speciation of the copper (*vide infra*). We then evaluated the antibacterial potential of both the TAPILs and the dual-modal composite solutions.
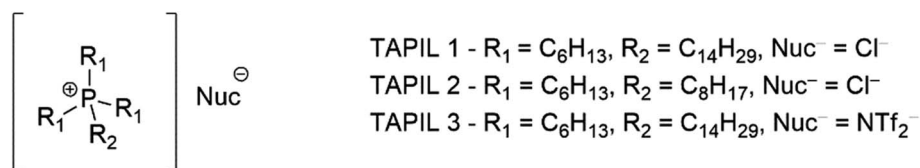

Fig. 1 The chemical structures of the three TAPILs used in this study.

TAPIL 1 - R$_1$ = C$_6$H$_{13}$, R$_2$ = C$_{14}$H$_{29}$, Nuc$^-$ = Cl$^-$
TAPIL 2 - R$_1$ = C$_6$H$_{13}$, R$_2$ = C$_8$H$_{17}$, Nuc$^-$ = Cl$^-$
TAPIL 3 - R$_1$ = C$_6$H$_{13}$, R$_2$ = C$_{14}$H$_{29}$, Nuc$^-$ = NTf$_2^-$

2.2. Comparison of TAPIL anti-bacterial activities

The three TAPILs were screened against *E. coli* and *S. aureus* according to internationally recognized good laboratory practice standard procedures (Fig. 2). The bacteria were selected based on the required representative strains (Gram negative and positive, respectively) used for European Union regulations in the evaluation of disinfectants.[57–62] A standard resazurin-based assay was employed: a blue well indicates non-viable bacteria, while a pink one indicates viable bacteria. The MIC and the MBC values are summarized. The data is visually extremely clear: these three TAPILs have widely varying antibacterial properties—*N*-bis-triflimide **TAPIL-3** does not show any anti-bacterial effects even at concentrations as high as 2 mg mL^{-1}. **TAPIL-1** shows bacteriostatic properties at intermediate concentrations, while **TAPIL-2** prevents *E. coli* proliferation at concentrations at least as low as $\sim$4 µg mL^{-1}. The effective concentration could not be determined from this initial scan as our concentration scan does not go low enough. These values are in broad accordance with expectations.[25] The length of the alkyl substituents on the TAPIL play an important role in determining the anti-microbial properties of the TAPIL: butyl to octyl cationic groups have been found to be more strongly bactericidal, as expressed by low MBC values.[42,46,47] For *E. coli*, the bacteriostatic and bactericidal effects are known to overlap somewhat.[63] In our case, **TAPIL-2**, with three hexyl and one octyl chains, has greater efficacy than **TAPIL-1**, bearing three hexyl chains and one tetradecyl group. The

chloride being more effective is also consistent with the literature as TAPIL-halides are previously reported to have anti-microbial properties.[40] The presence of one longer alkyl chain on the central phosphorus is deemed essential for anti-microbial activity since symmetrical TAPILs with four identical alkyl substituents around the phosphorus atom are likely to interact less strongly with the cell membrane to induce cell death.[45,47,64–67] Surprisingly, exchange of the halide for the less coordinating triflimide resulted in the abrogation of the anti-microbial activity of **TAPIL-3**. In alkyl-imidazolium ILs, the nature of the anion including its chaotropicity exerts practically no effect on anti-microbial activity of the ILs;[65] this is not our observation for TAPILs. Finally, we monitored the MIC/MBC values of **TAPIL-2** over a period of 3 weeks upon ambient storage open to the atmosphere. We did not notice any change in its antimicrobial activity.

2.3. Characterization of TAPIL/Cu NP composites

2.3.1. UV-visible spectroscopy. Metallic NPs show characteristic UV-visible absorption bands, often indicative of the size, the shape, and the composition of the NPs; these can be compared with the CuCl simply suspended in the TAPIL to show conversion (Fig. 3).[68]

CuCl is a white powder that turns **TAPIL-2** (clear and colourless when neat) pale yellow upon dissolution. The absorption band for CuCl in **TAPIL-2** can consequently likely be attributed to a complex of the type $[PR_3R']_n^+ [CuCl_{(n+1)}]^{n-}$.[69] The

(a) Concentrations (µg/mL) / Control
(b) Concentrations (µg/mL) / Control

(c)

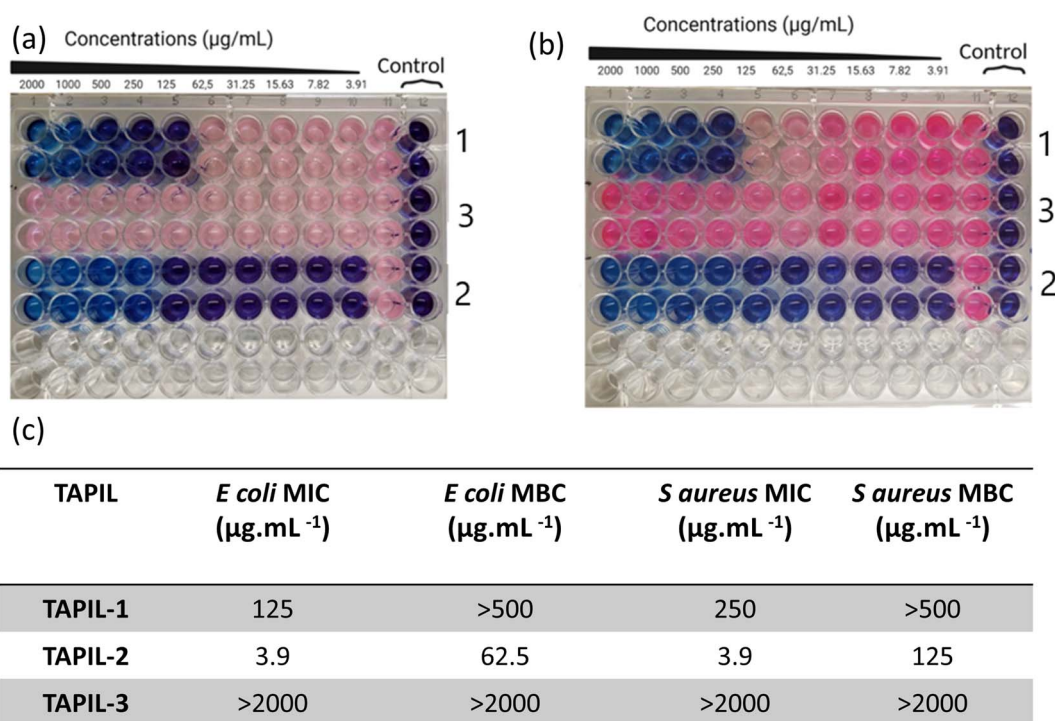| TAPIL	*E coli* MIC (µg.mL^{-1})	*E coli* MBC (µg.mL^{-1})	*S aureus* MIC (µg.mL^{-1})	*S aureus* MBC (µg.mL^{-1})
TAPIL-1	125	>500	250	>500
TAPIL-2	3.9	62.5	3.9	125
TAPIL-3	>2000	>2000	>2000	>2000

Fig. 2 MIC evaluation of the three TAPILs with *E. coli* (a) and *S. aureus* (b) as the microorganism under study, using resazurin as an indicator of bacterial viability. The numbers on the right correspond to the TAPILs – *i.e.*, "1" stands for **TAPIL-1**; (c) MIC and MBC values recorded for the three TAPILs deployed against *E. coli* and *S. aureus* as archetypal representative microorganisms.
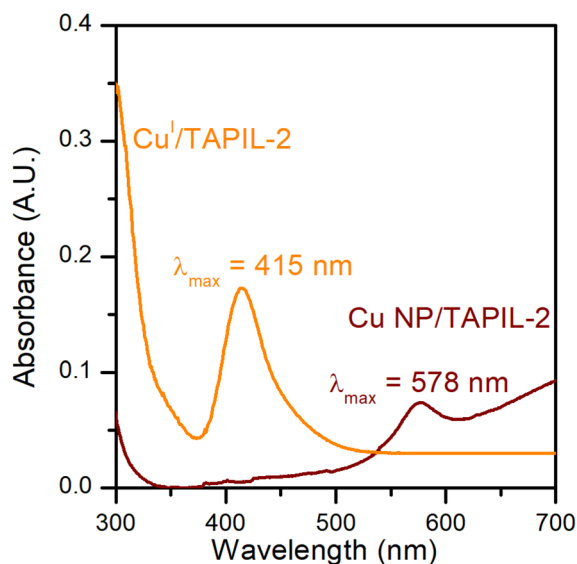
Fig. 3 UV-visible spectra of Cu(I)Cl and Cu NPs in TAPIL-2.

absorption band of Cu NPs in **TAPIL-2** is consistent with previous reports showing Cu NPs surface plasmon resonance bands in the range 520–580 nm.[37,70]

2.3.2. Electron microscopy of composite-2 (TAPIL-2/Cu NP). Both SEM and TEM (Fig. 4) were used to image the composites, although this was rendered exceptionally difficult by the fact that the TAPIL forms a sticky, protective coating

around the NPs. In the SEM images, we can observe grape-like clusters of NPs conjoined to each other, rather than isolated NPs suitable for detailed size and shape analysis using high-resolution images.

TEM at higher resolutions, as well as high-angle annular dark-field imaging (HAADF), were used to examine Cu NPs formed within the TAPIL matrices. As Fig. 4(c) reveals, they are still prone to forming clusters, even at high dilutions. From Fig. 4(d), we can conclude that the Cu NPs are highly polydisperse in terms of size distribution. This is not unusual for metallic NPs generated *in situ* within IL matrices.[36,38,52] The average size of the Cu NPs in **composite-2** was found to be 9.6 ± 5.2 nm, although some larger aggregates were not taken into consideration while performing these measurements. It is to be noted that during TEM sample preparation, **composite-2** is heavily diluted in an organic solvent containing dissolved oxygen, and sonicated, likely leading to considerable NP size reduction through the oxidative attrition mechanism that we mention in the following sections. Thus, Fig. 4(d) shows Cu NPs to be much smaller than they were initially [Fig. 4(a) and (b)]. The size distribution profile of the Cu NPs associated with Fig. 4(d) may be found in the ESI (Fig. S7†).

2.4. Temporal changes in Cu speciation within the composites

ILs stabilize metal ions in unusual oxidation states, as well as stabilizing very small sub-nm metallic clusters. Au NPs in
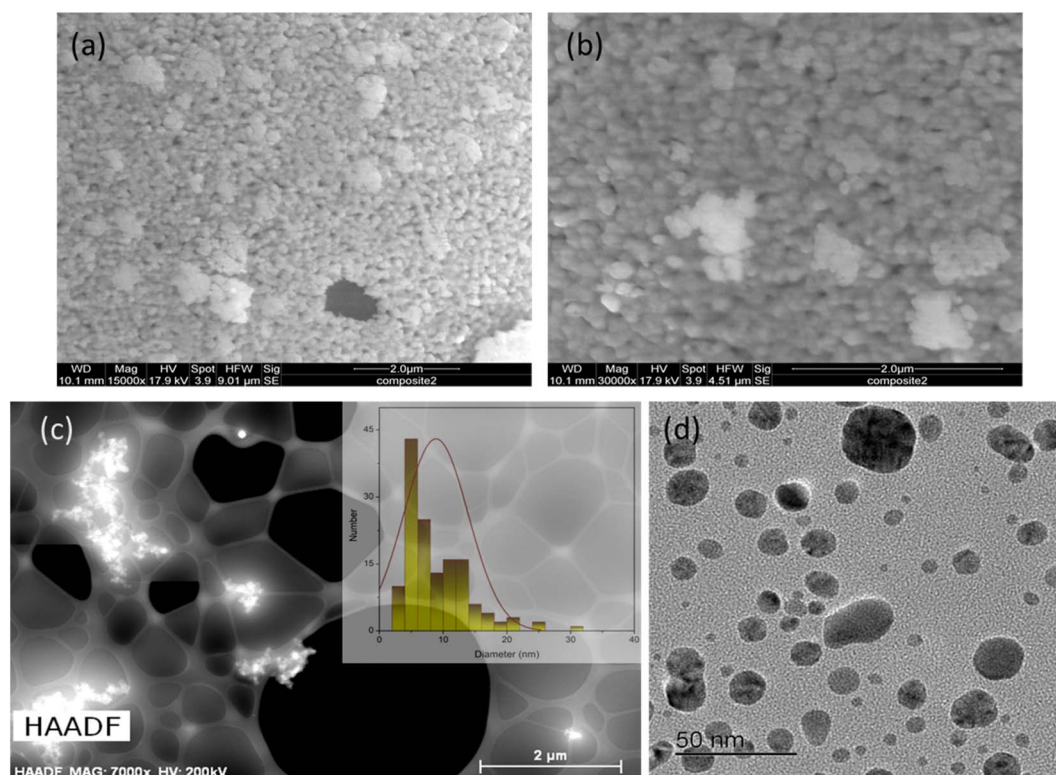

Fig. 4 SEM of **composite-2** (TAPIL-2/Cu NPs) at increasingly higher resolutions. In (b), it is possible to make out individual NPs within the clusters. (c) HAADF-TEM of TAPIL-2/Cu NPs, showing clusters (inset – Cu NP size distribution profile); (d) HR-TEM of the composite material showing Cu NPs.

TAPILs in the presence of oxygen oxidize to Au(I) and then to Au(III);[37] similarly, Fe NPs in alcohol or water are protected from oxidative dissolution by a thin layer of passivating FeO_x on the surface, while in TAPILs, they oxidize to soluble $Fe(III)Cl_x^{(x-3)-}$ species.[39] Maier and co-workers found that metallic Cu, Ag, and Au foils showed considerable mass loss after exposure to $[C_6C_1Im][Br_2I]$ for 6 h at 40 °C; XPS was used to determine the final oxidation states of the dissolved metallic species. It was determined that only the monovalent ions [Au(I), Ag(I), Cu(I)] were formed.[71] Recently, Vicente et al. studied the "dissolution" of bulk Fe, Cu, Ni, Co, and Zn in [BMIM]Cl, and concluded that the dissolution happened through oxidation to soluble salts.[72] Similarly, there are many examples of polynuclear metal clusters within IL matrices[73]—for example, elemental bismuth and bismuth(III) cations synproportionate in the ionic liquid [BMIM]Cl/AlCl$_3$ within minutes to form bismuth polycations (such as $Bi_5(AlCl_4)_3$) in situ.[74] While there is a vast body of work on Cu NPs in water as potential antimicrobial species, very little of it is relevant to TAPILs, where copper speciation is understudied.

We acquired the normalized Cu K-edge XANES spectra of Cu metal foil, CuO, Cu_2O, and the three composites, either freshly opened, or after 24 h of exposure to air (Fig. 5). Cu foil exhibits a rising-edge transition (4p ← 1s) at 8981.0 eV, while this feature is shifted to 8981.5 eV and 8985.5 eV, for Cu(I) oxide and Cu(II) oxide respectively.[75,76] All three freshly opened composite samples display a similar rising-edge at around 8981 eV, indicating their mixed oxidation state nature [Cu(0) and Cu(I)]. The spectra recorded after 24 h show similar features, but they resemble Cu(I) more closely, indicating slow oxidation of Cu(0) over time to Cu(I), but not to Cu(II), over the period of study.

We then compared the ensemble average oxidation state of copper (δ-Cu$_{av}$) in the composites as a function of copper K-edge energy shift (Fig. 6), using the method of Sargent et al.[77] The oxidation states for Cu within the composites at $t = 0$ are close to, but not exactly, zero. This indicates either incomplete reduction, or that the slow oxidation of Cu(0) to Cu(I) has already begun; after 24 h of exposure to air, the oxidations states increase progressively to values closer to +1. It is noted that the composite containing the N-bis-triflimide anion actually contains almost all of its Cu in the zero valent state to begin with, and only shows a small increase at $t = 24$ h. In general, we can conclude that at $t = 0$, all the composites have oxidation states closer to 0; they then undergo slow oxidation over 24 h, approaching +1 oxidation states. It is to be noted that we do not know if the NPs release individual copper ions or small copper
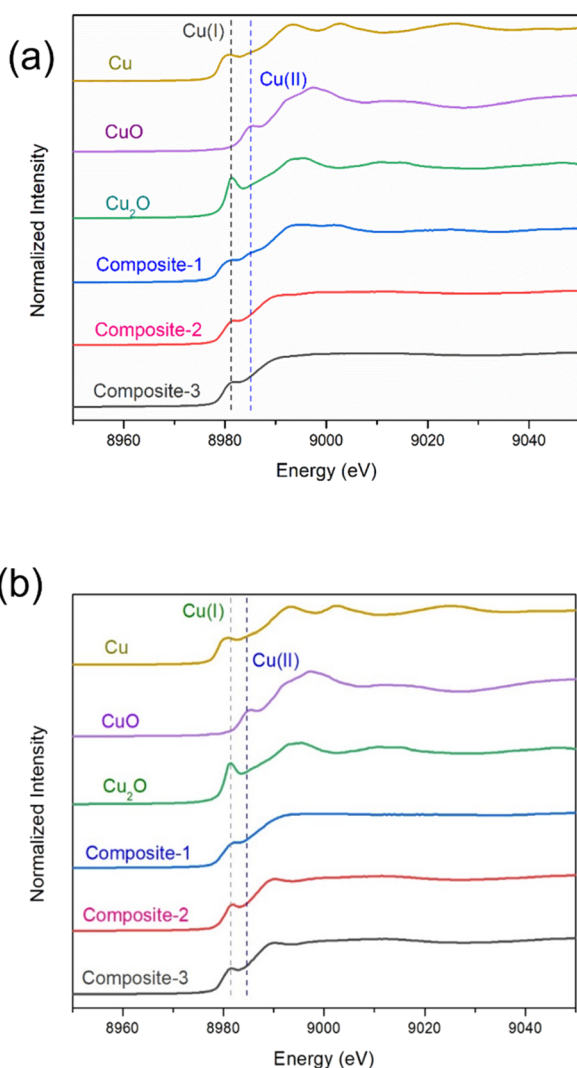

Fig. 5 XANES of the three composites immediately upon exposure to air (a), and 24 h of exposure to air (b). Cu(0), Cu(I), and Cu(II) standard spectra are also shown.
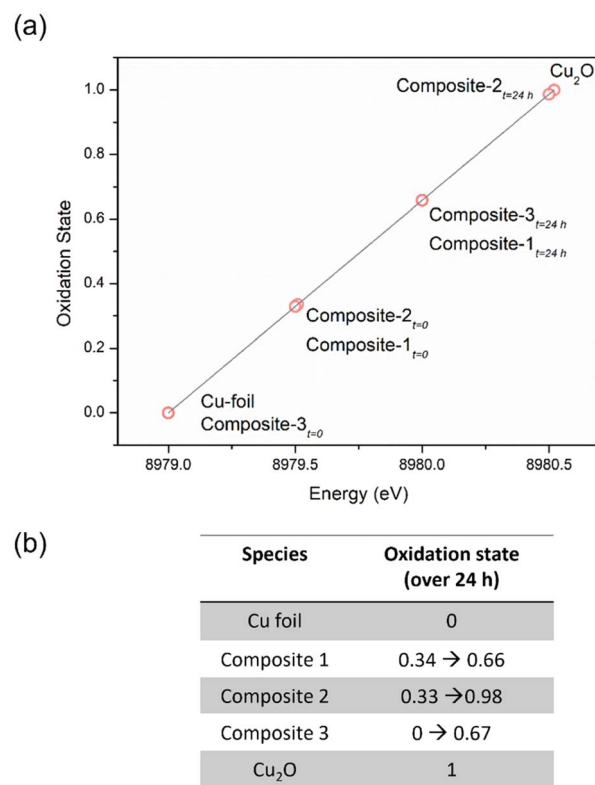

Fig. 6 The average oxidation state of copper in the ionic liquid sample based on energy shift function represented graphically for a period of 24 h (a), and tabulated (b).

Species	Oxidation state (over 24 h)
Cu foil	0
Composite 1	0.34 → 0.66
Composite 2	0.33 → 0.98
Composite 3	0 → 0.67
Cu_2O	1

clusters over time, since the measured oxidation states are ensemble averages.[78] However, within TAPIL matrices, Cu NPs do "fall apart" over time, releasing charged species that may have catastrophic effects on microorganisms.

2.5. Anti-bacterial activities of composites 1, 2, and 3 against *E. coli* studied as a function of storage time

If only the freshly made composite is active, this is useless. Consequently, we studied the anti-bacterial activities of **composite-1** and **-2** over time. **Composite-3**, like the parent TAPIL, did not show any anti-bacterial activity after formation and was eliminated from the tests. Both **composite-1** and **-2** were bactericidal, with MIC/MBC values in the tens of μg mL^{-1} for the former, and in the order of 10^{-2} μg mL^{-1} for the latter. Thus, **composite-2** is a better weapon against *E. coli* by orders of magnitude compared to **composite-1**. Some of this enhanced activity in comparison with the base TAPIL could no doubt be attributed to the presence of the Cu NPs within the TAPIL matrix, which are known to have antimicrobial properties, although activity from residual lithium and aluminum salts cannot be completely ruled out. According to relevant *E. coli* literature, the MIC of Li$^+$ is *ca.* 200 mM, and that of Al$_2$O$_3$ NPs is in the range of 1600–3200 μg mL^{-1}; it is unlikely, therefore, that these adventitious species will be so highly antimicrobial at the low concentrations in which they are present within our composites.[79-81] Also arguing against the possibility of lithium and aluminium salts being the 'real' antibacterial species is the lack of activity for **composite-3**; if the salts were independently highly cytotoxic, they would affect this mixture as well. We attempted 'traceless' Cu NP incorporation (*i.e.*, incorporation of only Cu NPs without any reaction byproducts) within TAPILs by adding Cu NPs synthesized in water through a literature protocol[82] to **TAPIL-1** and **-2**; residual water was then removed under reduced pressure and mild heating. Unfortunately, the pre-formed Cu NPs were simultaneously oxidized, as demonstrated by XANES (data not shown), as well as through a visually observable color change from reddish pink to yellow.

These results, though not unexpected, indicate higher-than-anticipated levels of synergy between two orthogonal antimicrobial mechanisms. What we did find noteworthy is the temporal evolution of the antibacterial activity of the active composites. For many bactericidal materials, the MIC and MBC values increase over time, indicating loss of anti-bacterial activity owing to API degradation.[83] Kuznetsov and colleagues, examining Cu NPs and Cu(II) ion suspensions, demonstrated that storage time was an important factor for determining the antimicrobial properties. The cytotoxicity of small (50 nm) Cu NP suspensions fell after 24-hour storage, while the antibacterial activity of 100 nm Cu NP suspensions displayed no such time dependence; however, this observation was not universal across all NP concentrations.[84] At concentrations under 1 mg L^{-1}, Cu(II) ions do not demonstrate significant toxicity to *E. coli*; at higher concentrations, they do show significant antibacterial activity. Small NPs have smaller surface areas, which potentially interferes with the rate of copper ion release owing to more facile formation of passivating copper oxo-hydroxide

layers on the NP surface, and consequently reducing activity at concentrations under 1 mg L^{-1}. At higher concentrations, no lowering of antibacterial activity was recorded for the 50 nm Cu NPs, presumably due to the sustained higher concentration of released Cu(II) ions from the many more degrading NPs, in spite of any passivating layers that may or may not be formed on the NP surface.

In our systems, however, there is a downward trend for MIC/MBC values over storage time, especially for **composite-1**. We also note that unlike a 24-hour storage time, we are resting the particles for weeks (Fig. 7). Within the **TAPIL-1** and **TAPIL-2** matrices, Cu NPs slowly disaggregate over time, releasing charged species (such as Cu(I) ions and/or charged Cu clusters); these charged fragments then annihilate microbes that encounter the composites. The longer the material is stored, the greater the exposure to ambient oxygen, and the faster the disintegration of the Cu NPs which serve merely as reservoirs for copper ions. This is in accordance with the findings of Bastos
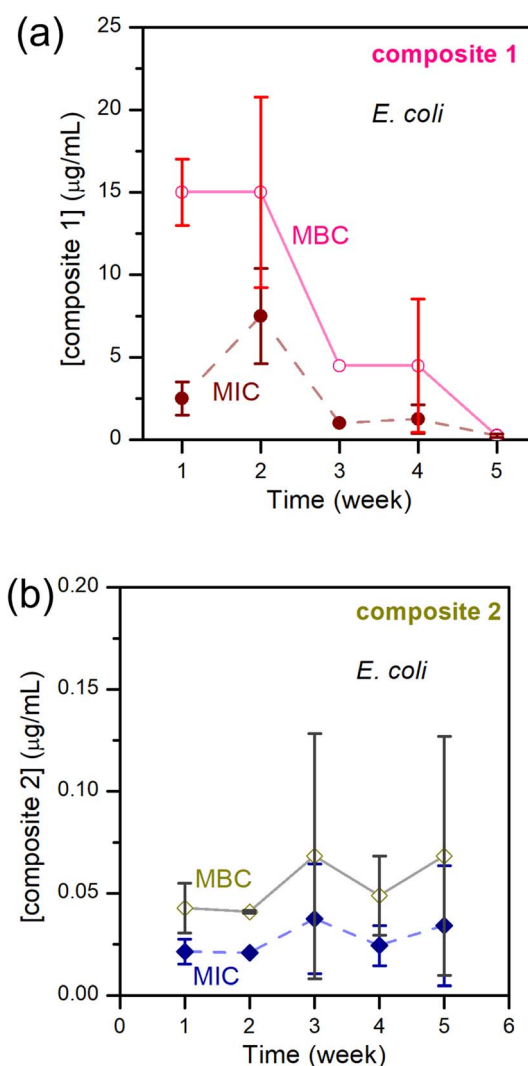

Fig. 7 MIC and MBC of *E. coli* – (a) upon exposure to **composite-1**; (b) upon exposure to **composite-2**; over 5 weeks.

et al., who demonstrated that release of copper ions from Cu NPs is chiefly responsible for their antibacterial effects.[85]

Keeping this hypothesis in mind, it is very easy to correlate δ-Cu_{av} with the antibacterial activities of the composites. In **composite-3**, δ-$Cu_{av} = 0$, and the TAPIL itself possessed no antibacterial properties, so no bactericidal activity was noted for the composite as a whole. Comparing composites **1** and **2**, the latter contained the more antimicrobial TAPIL. **Composite-2** also showed greater change δ-Cu_{av} over 24 h, indicating enhanced release of charged copper species. It is also the most anti-bacterial composite on our list. The relatively slower oxidation of the Cu NPs in the presence of **TAPIL-1** may be related to the fact that it has a longer alkyl chain (C_{14} as opposed to C_8) which might offer better protection against oxidative decomposition to the Cu NPs enclosed within the TAPILs.

2.6. Exploration of the anti-bacterial activity of composite-2 through a bacterial panel test

A 'panel test' was performed to evaluate the antibacterial activity of **composite-2** against a number of pathogenic bacteria. The bacteria tested included one Gram positive [*Staphylococcus aureus* (ATCC 6538)] and six Gram negative [*Acinetobacter baumannii* (ATCC 19606), *Escherichia coli* K12 strain (ATCC 10798), *Escherichia coli* (ATCC 10536), *Salmonella enterica* subsp. *enterica* serovar Typhimurium (ATCC 13311), *Escherichia coli* (ATCC 13706), and *Pseudomonas aeruginosa* (ATCC 10145)] bacterial species of concern (Fig. 8 and S5† replots the logarithms of these values). The order of efficacy of **composite-2** in terms of its bactericidal effect varies depending upon the bacterial strain, but for all tested strains, MIC and MBC recorded were of the order of 0.1–0.01 μg mL^{-1}. The most "resistant" bacteria proved to be *P. aeruginosa*, an encapsulated, Gram-negative, rod-like

Fig. 8 Bacterial panel test results for **composite-2**.

bacterium that is known for becoming multidrug resistant.[86] The most susceptible bacterial species was *S. aureus*, a Gram-positive spherical bacterium. The ratio of MBC/MIC was used to characterize the antimicrobial activity; when the ratio of MBC/MIC ≤ 2, the composite was considered to be bactericidal; for a ratio ≥4, it was defined as being bacteriostatic.[87] Based on the MBC/MIC ratio, **composite-2** was designated bacteriostatic for *A. baumanii*, whereas for all other bacteria, it was bactericidal. In general, ILs are better at destroying Gram-positive bacteria in comparison with Gram-negative bacteria due to the thicker and more lipophilic cell membranes of the Gram-positive bacteria,[66] whereas Cu NPs are known to be effective against both types of bacteria.[88] Since our composite contains both these materials, it is unsurprising that it has broad spectrum activity.

2.7. Exploration of the anti-bacterial activity of TAPILs and composites using SEM

We designed additional SEM experiments to observe the effect of exposure of *E. coli* to the TAPILs, as well as to the composites created from the TAPILs. Details of sample preparation for these experiments may be found in the relevant Experimental section. The SEM images are shown in Fig. 9.

The proposed mechanism of action of the composites involves the copper ions released from Cu NPs absorbing onto the bacterial cell surface, damaging the cell membrane, hampering their replication process, and inducing cell death.[85] Redox reaction cycles involving Cu (0), Cu(I), and Cu(II), analogous to the Fenton reaction,[89] have been known to occur on the surface of bacterial cells.[90] This produces peroxides, which are known to compromise the cytoplasmic membrane. We expect composites **1** and **2**, to show significant redox activity (*vide supra*), so this pathway is likely active in our system. Copper ions also impact the permeability of the cell membrane, leading to cellular damage. We have already demonstrated that our composites release copper ions, especially upon exposure to ambient air.[37] From these results, it is believed that binding of copper ions to the bacterial cell surface plays an important role in bactericidal activity of our composites. However, this activity does not take place in a vacuum. It is occurring in a cell-penetrating IL.

The effect of ILs on bacteria has been reviewed recently.[66] The major pathways for bacterial damage induced by ionic liquids include: (i) sorption onto the cell surface; (ii) deactivation of bacterial membrane proteins and electrostatic interaction of the IL molecule with membrane phospholipids; and finally (iii) cell penetration, formation of physical pores, leakage of intracellular cytoplasm, and cell lysis. We can follow this process through imaging.

SEM micrographs of untreated *E. coli* show clusters of rod-shaped cells with relatively smooth surfaces, indicating the integrity of the bacterial membrane (Fig. 9(a), also see inset). After 18–24 h of incubation with **TAPIL-2** at concentrations slightly below MIC, the cells seem to lose their membrane integrity, with some visible cavities in the cell walls. Meanwhile, some of the cells in Fig. 9(b) and (c) present numerous tears or
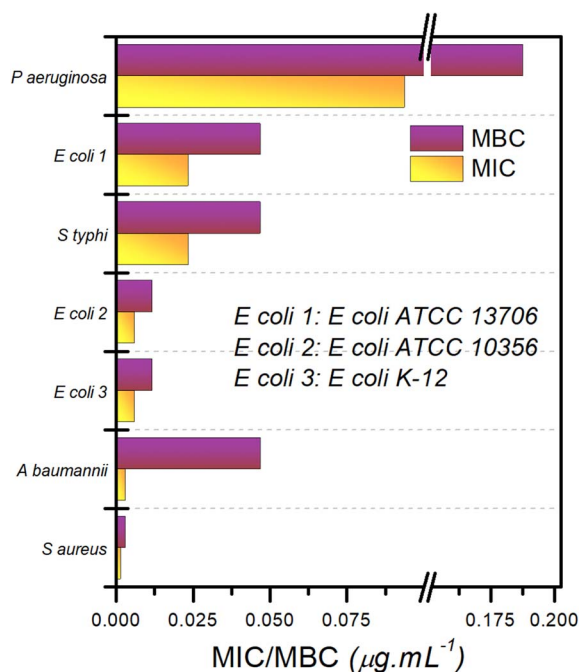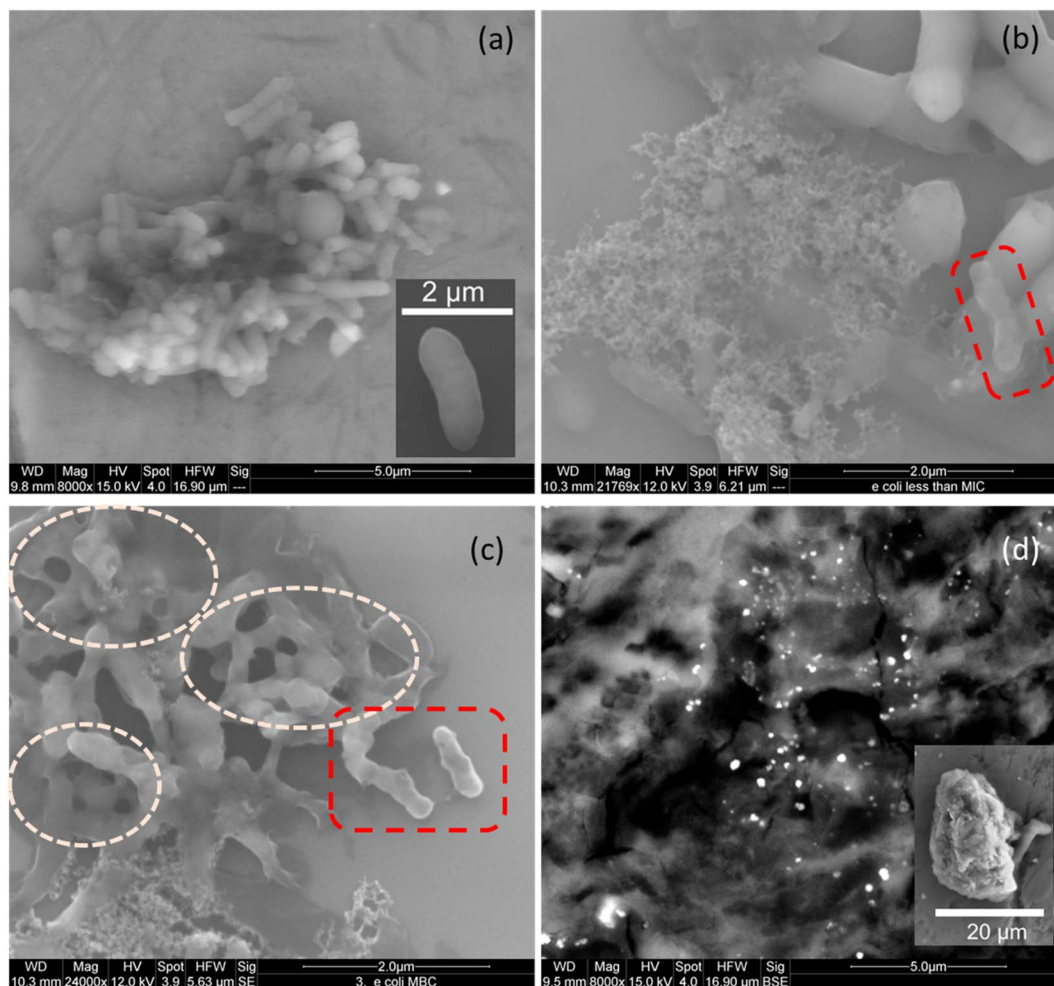
Fig. 9 SEM images of *E. coli* – (a) without exposure to TAPILs or composites; (b) upon exposure to $\sim$3 µg mL^{-1} (sub-MIC) of **TAPIL-2**; (c) upon exposure to $\sim$65 µg mL^{-1} (>MBC) of **TAPIL-2**; (d) upon exposure to $\sim$0.1 µg mL^{-1} (>MBC) of **composite-2**. The ochre dashed circles highlight damaged bacterial membranes, while the red dashed boxes show thin, shriveled bacterial cells.

ruptures in their cell walls. This is likely due to the TAPILs irreversibly compromising bacterial cell membrane permeability and creating pores.[91] The rupture of the cellular membrane can lead to leakage of essential solutes, thus producing a shriveled, indented appearance of *E. coli* cells, which have been highlighted in broken red boxes in Fig. 9(b) and (c). Furthermore, we can also see collapsed *E. coli* cells in Fig. 9(b), spilling cellular debris.

The most catastrophic effects on *E. coli* cells were obtained upon exposure of the cells to **composite-2** at a concentration slightly above the MBC (Fig. 9(d)). Cells were annihilated, and no surviving *E. coli* cells were found despite repeated attempts at imaging; only spilled cellular material could be seen. The Cu NPs within the composites showed up as bright dots amidst the bacterial detritus. These results seem to indicate that direct damage to the cytoplasmic membrane of the *E. coli* cells, owing to strong interactions between the membrane and the composites, elicits cell death. A close-up SEM micrograph of a few highly damaged *E. coli* cells (with tiny remnants of rod-like cellular structure, but with almost the entirety of the enclosed

cellular material spilling out) can be seen in the inset of Fig. 9(d), as well as in Fig. S7 in the ESI.†

The bacterial cell wall is a 7–8 nm thick peptidoglycan layer made up of glycan chains of alternating *N*-acetylglucosamine and *N*-acetylmuramic acid residues, which are cross-linked by short peptide chains. A bilaminar structure of tightly packed phospholipids and lipopolysaccharides containing membrane proteins form an outer charged layer enveloping the peptidoglycan membrane.[92] By comparing our SEM micrographs with similar ones in the literature,[93] we can conclude that electrostatic interaction between Cu-composites and membrane anionic phospholipids lead to the cytoplasmic membrane taking a 'direct hit'. This obviously compromises the integrity of *E. coli* cells, leading to cell perforation and death.[94]

2.8. Time kill kinetics assay for composite-2

Fig. 10 shows the time-dependent bactericidal activity of **composite-2** against *E. coli* and *S. aureus*. The results demonstrated a significant decrease in viable bacterial cell counts when exposed to **composite-2** at the MIC, 2 × MIC (2-fold) and 4
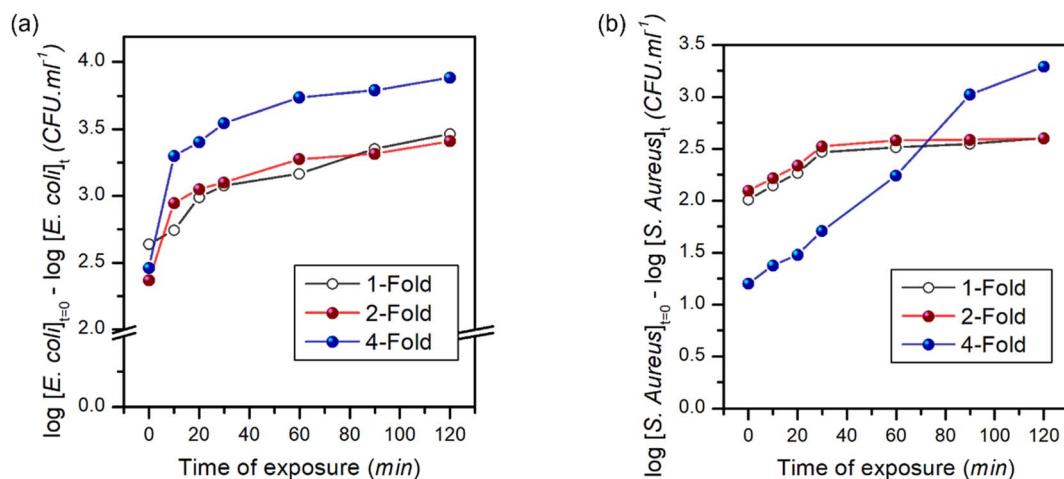
Fig. 10 Log reduction in concentration of viable bacterial cells plotted as a function of time of exposure to **composite-2** for three different **composite-2** concentrations; (a) for *E. coli*; and (b) for *S. aureus*.

$\times$ MIC (4-fold), indicating its antimicrobial performance. The relationship between **composite-2** concentration and exposure time on viable bacterial cells was explored using time-kill kinetics (Table S1†).[95]

Linear regression equations were obtained to analyze the relationship between time and viable cell counts, along with correlation coefficients to assess the strength of the associations. The killing kinetic assay demonstrated a time-dependent reduction in viable cell counts of both *E. coli* and *S. aureus* when exposed to **composite-2**. The log reduction values increased gradually over time, indicating a progressive bactericidal effect of the composite. After 10 min of exposure at the MIC, the log reduction for *E. coli* was 2.63, which increased to 3.46 at 120 min. Similarly, at the MIC *S. aureus* exhibited a log reduction of 2.14 at 10 min and 2.60 at 120 min. Regression analyses examined the relationship between exposure time and log reduction at different concentrations (Fig. 11). Exposure time
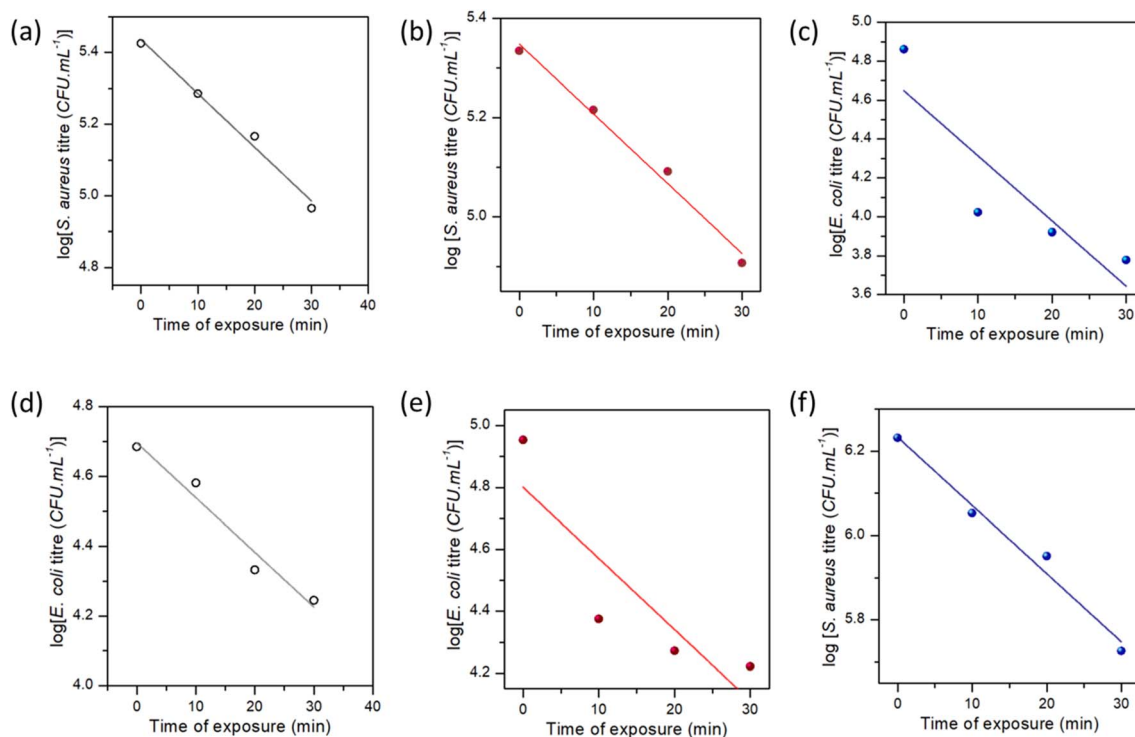

Fig. 11 Linear fit of the time kill kinetics data for *E. coli* (a)−(c) and *S. aureus* (d)−(f) upon exposure to **composite-2**. (Black hollow spheres = 1×; red solid spheres = 2×, and blue solid spheres = 4× MIC$_{composite-2}$.)

and log reduction for *E. coli* and *S. aureus* were found to be strongly correlated, indicating that prolonged exposure to **composite-2** led to a more pronounced decrease in viable cells.

We determined that Pearson's correlation coefficients ranged from -0.98113 to -0.88767 for *E. coli* and from -0.99355 to -0.99047 for *S. aureus*, with p-values < 0.05, highlighting the strength of the associations. The linear regression models explained a considerable portion of the variability in log reduction, as evidenced by the adjusted R-squared values ranging from 65.6% to 94.4% for *E. coli* and 97.2% to 98.2% for *S. aureus*. Regression analysis provided mathematical representations of the relationship between exposure time and log reduction in viable cells, reinforcing the effectiveness of **composite-2** in inhibiting bacterial growth.[96] Consistent patterns were observed across different fold levels in regression analyses. The strongest negative correlations were observed for the 1-fold reduction in *E. coli*, whereas *S. aureus* exhibited strong negative correlations across all log reduction levels. These regression models accounted for a significant proportion of the observed log reduction, as indicated by the high adjusted R-squared values for *E. coli* and *S. aureus*. The findings of the killing kinetic assay and regression analyses provides valuable insights into the time-dependent bactericidal activity of **composite-2** against *E. coli* and *S. aureus*.

3. Conclusion

Nanocomposites containing Cu NPs generated within TAPILs were tested for their antibacterial activity. Of the three TAPILs tested, P[6,6,6,8]Cl had the smallest MIC and MBC values against *E. coli*, while P[6,6,6,14]NTf$_2$ didn't show any bactericidal properties at all, even at elevated concentrations. Composites **1** and **2**, generated by the incorporation of Cu NP reservoirs synthesized by chemical reduction of copper salts dissolved in the TAPILs, showed slight increase in their antibacterial properties over time; this was explained using XANES to study the evolution of the oxidation state of copper within TAPIL matrices upon exposure to ambient air over time. **Composite-2** was shown to be bacteriostatic towards *A. baumanii* and bactericidal for a range of other bacteria, both Gram-positive and negative. SEM showed that while exposure to TAPILs on their own caused cracks and fissures to appear on bacterial cell walls, the composites caused total cell lysis, spilling cellular debris, and annihilating the bacteria. This can be thought of as a two-stage warhead. Both the copper and the IL increase permeability, together they rip the cell open, and both show antimicrobial activity on the cellular contents should they get inside. This is a very potent combination. The progressive reduction in viable cell counts and the strong negative correlation between exposure time and log reduction indicate the effectiveness of **composite-2** in inhibiting bacterial growth over time. Regression analyses further supported the concentration- and time-dependent bactericidal effects of **composite-2**. Returning to the need for sustainability, we need highly active agents. Bleach is highly active, but one needs on the order of one gallon of concentrated bleach/10,000 gallons of water to sanitize. Although this would be an unlikely

application for TAPILs (compared to industrial sanitation), for the sake of comparison with a familiar example to show relative efficacies, we can compare the amount of bleach and **composite-2** required to sanitize an Olympic swimming pool (660 000 gallons, 2.5 million kg). Approximately 1 gallon of concentrated bleach is recommended per 10 000 gallons to be reasonably bacteriostatic. This implies 66 gallons of concentrated bleach are needed (250 kg); in comparison, **composite-2** is lethal to *E. coli* at 0.05 mg L^{-1}. This implies that 125 g of **composite-2** would be sufficient for the same volume. This is 2000 times less material.[97] It is also important to note that the activity is due to the synergistic activity of the IL and the CuNPs; this synergy would be lost upon further dilution as they separate. In the introduction, we discussed the limited work done to date on the environmental toxicology of phosphonium ionic liquids and noted that at 100 mg L^{-1} medium chain phosphonium ILs were safe for zebrafish embryos, and at 1 mg L^{-1} longer-chain phosphonium ionic liquids were reasonably safe. The effective concentration of our material is 20-fold lower than this concentration. Further evaluation is needed, but it is likely that the concentration of this reagent will be very low in the environment should it be deployed; bioaccumulation or even environmental accumulation of this material will need to be considered as it does appear that phosphonium salts do have slower biodegradation than other materials. This novel class of antibacterial materials is being investigated further both to address these concerns, and for the creation of germicidal coating materials for surfaces and further optimization of the formulation is under way.

4. Experimental

4.1. Materials

The TAPILs were purchased from Strem Chemicals. The copper salts were purchased from Oakwood Chemical. LiAlH$_4$, glutaraldehyde, resazurin sodium salt, and dimethyl sulfoxide (DMSO) were purchased from Sigma-Aldrich, Germany. Organic solvents, HPLC grade water, and Mueller Hinton Media from Millipore Sigma, Germany were used throughout the study. HEPES buffer was purchased from Bio Basic Inc., Canada.

4.2. Instruments

4.2.1. UV-visible spectroscopy. UV-visible spectroscopy was performed on diluted samples (*ca.* (1 : 25), THF). The TAPIL dissolved in THF was used as the background. An Edinburgh Instruments DS5 spectrophotometer was used for the collection of spectra. Samples were loaded in standard 10 mm capped quartz cuvettes.

4.2.2. SEM. Freshly prepared Cu NP/TAPIL composites were smeared onto freshly cleaned smooth silicon wafers, most of the smeared material removed with a KimWipe™, and immediately imaged in high vacuum using a FEI Quanta 200 Environmental Scanning Electron Microscope (ESEM) fitted with an EDAX Octane Plus SDD detector.

For bacterial samples, the following sample preparation protocol was employed. 50 μL each of *E. coli* and *S. aureus* at 10^5

CFU mL^{-1} in the stationary phase were set up for microplate dilution with serially diluted 50 μL of **TAPIL 1** and **TAPIL 2** with 50 μL of MHB in 96-well culture plates for 24 h at 37 °C. 1 mL of a mixture at different composite concentrations (control, sub-MIC, MIC, MBC, slightly greater than MBC) was transferred into a 2 mL centrifuge tube and centrifuged at 1000 rpm at 4 °C for 5 min, and the supernatant was then aspirated. The precipitate was resuspended with 0.1 M HEPES and recentrifuged thrice; the supernatant was gently aspirated and removed. The pellet was then fixed in 2.5% glutaraldehyde, a primary fixative, incubated at room temperature for 30 minutes, and left overnight. The pellet was then resuspended in 0.1 M HEPES buffer four times for 15 min, collecting the pellet through centrifugation followed by aspiration after each iteration. Finally, the pellets were washed with distilled water twice to remove the buffer. The pellet was then dehydrated by treatment with acetone at gradually increasing concentrations (50%, 70%, and 90% each for 15 min, 100% twice for 20 min). Finally, the pellet was incubated in 100% acetone for 2 h. Subsequently, the sample was drop-cast onto a smooth, clean silicon wafer, allowed to dry, and observed under the SEM.

4.2.3. TEM. An FEI Tecnai Osiris S/TEM system equipped with Bruker SuperX EDX detectors and operated at 200 keV was used for TEM. Samples were diluted in diethyl ether and sonicated, followed by drop-casting onto lacey formvar Cu 200 mesh grids. NP sizes were determined using ImageJ with an average of at least 100 NPs from multiple images.

4.3. Handling of TAPILs

TAPILs were dried under vacuum at 60 °C for 6–8 h prior to usage. ^{1}H and ^{31}P NMRs were recorded to rule out the presence of NMR-detectable amounts of impurities such as unreacted phosphines. The NMR data may be found in the ESI (Fig. S1–S3†).

4.4. Preparation and storage of the composites

In a representative synthesis, Cu NPs were generated directly within **TAPIL-1** as follows: to 10 mL of **TAPIL-1** in a Schlenk flask at 70 °C under N$_2$, CuCl (~3 mg; [Cu] = ~380 μg mL^{-1}) was added, and vigorously stirred to give a pale-yellow solution. The environment within the Schlenk flask was exchanged with nitrogen thrice, alternating with vacuum. The solution was cooled to 60 °C, and a stoichiometric excess of LiAlH$_4$ reagent (1.5 mL, 1 M in THF) was injected dropwise over a period of 5 min. Rapid effervescence followed, and the entire solution turned reddish-brown, indicating Cu NP formation (Fig. S4†). After the addition of LiAlH$_4$, volatile impurities were removed by vacuum stripping the system at 80 °C for 0.5 h. The Cu NP/TAPIL composites thus obtained were stored under N$_2$ in capped vials until use. The vials were kept in an ordinary refrigerator at 4 °C.

4.5. Biological procedures

4.5.1. Evaluating MIC and MBC of materials. *Staphylococcus aureus* (ATCC 6538), *Acinetobacter baumannii* (ATCC 19606), *Escherichia coli* K12 strain (ATCC 10798), *Escherichia coli* (ATCC 10536), *Salmonella enterica* subsp. *enterica* serovar Typhimurium (ATCC 13311), *Escherichia coli* (ATCC 13706), and *Pseudomonas aeruginosa* (ATCC 10145) were employed for *in vitro* antimicrobial testing. The new cultures of all the bacteria used were grown at 37 °C for 24 h in an incubator. The inoculum of ~10^6 cells were taken from overnight culture following the CLSI recommendation. 0.015 g of resazurin was then dissolved in 100 mL of 1× PBS and filter sterilized to make a 0.015% (w/v) resazurin solution for a redox reaction. The material being analyzed for anti-bacterial activity—TAPIL or composite—was dispersed in Mueller Hinton Broth (MHB), with 0.3% DMSO as an emulsifier. The CLSI M100-S25 standard microdilution was employed to determine the minimum inhibitory concentration (MIC) and the minimum bactericidal concentration (MBC) of materials under investigation. The MIC was determined with different dilutions of the composites, their concentrations ranging from 2.5–9.77 × 10^{-3} μg mL^{-1} in MHB. The initial concentration of the bacteria (1 × 10^8 CFU mL^{-1} at an optical density 0.150 at 620 nm) was diluted to 1 × 10^6 CFU mL^{-1}, and this was used as the standard inoculum. The positive control used in this study comprised of only the bacterial suspension in MHB. In contrast, the negative control consisted of the medium sterility MHB without bacterial suspension and the DMSO for the solvent sterility without composites or bacterial suspensions. In a representative experiment, 150 μL of the material under examination (2.5 μg mL^{-1}) was poured in the first well of column 1. Subsequently, columns 2–10 was filled with 50 μL of MHB. 50 μL of the mixture of the test composite in well 1, column 1 was serially transferred to column 2 up to column 10 using a multichannel pipette to achieve a serial 2-fold dilution of the ionic concentration (2.5–9.77 × 10^{-3} μg mL^{-1}). Afterwards, 50 μL of the standardized inoculum was added to columns 1–9. Then, column 10 was then filled with 100 μL of the standardized inoculum as positive control and, column 11 with 100 μL of DMSO, column 12 for MHB for the growth control and broth sterility control, respectively. The plate was incubated for 24 h at 37 °C. After the incubation, 30 μL of the redox dye resazurin was added to all the wells and incubated for 2 h to observe the colour change from blue to pink. The colour change is due to the reduction of resazurin to resorufin by viable bacteria cells. After 2 h of incubation, all the wells that retained the blue colouration of resazurin were scored as above the MIC. The first well with no change in colour was chosen as the MIC. The remaining unchanged wells were plated directly on the MHA (Mueller–Hinton Agar plates) to determine the minimum biocidal concentration (MBC). MIC and MBC values were recorded by counting the number of colonies. The assay was duplicated in the 96-well plate and repeated three times with three newly independent grown cultures for inoculum preparation and standardization.

4.5.2. Time study of composites against *E. coli*. The temporal evolutions of the antibacterial properties of composites **1** and **2** were tested over a period of 5 weeks. Every week, the MIC and MBC of the composites were determined against *E. coli* as a representative microorganism. The assay was conducted in triplicate. The procedure was the same as the microdilution protocol for evaluating MIC and MBC (*vide supra*). Between

testing periods, the composites were stored in the fridge in capped vials and underwent a slow change in colour from deep opaque reddish-brown to almost completely transparent, with a very faint tinge of yellow (week 3–4).

4.5.3. Kinetics of *E. coli* and *S. aureus* killing by composite-2. Time-killing assays for describing the kinetics of antibacterial action of **composite-2** against two bacterial species were conducted based on a protocol reported by Li and coworkers. A suspension test was conducted with the 1×10^7 CFU mL^{-1} of bacterial test suspension from overnight culture with MHB. **Composite-2** concentrations were 1×, 2×, and 4× MBC. 0.5 mL of the suspension mixture was incubated at 37 °C with gentle agitation in a shaking water bath. Exposure time points selected were between 0 and 120 min of incubation. 10 mL of the suspension was serially diluted and inoculated on agar plates. The viable bacteria colonies were enumerated after 48 h of incubation at 37 °C. All the tests on time-kill kinetics were conducted in triplicates.

4.6. X-ray absorption spectroscopy

All X-ray absorption spectroscopy (XAS) measurements were conducted at the Canadian Light Source (CLS). Cu K-edge XANES were acquired at the BIOXAS beamline (071D-2M), which is equipped with a Si(220) double-crystal monochromator ($\phi = 0°$). Data were collected using a Canberra 2 × 32-element HPGe solid-state detector. The copper foil was utilized as an in-line reference for energies at the Cu K-edge. Liquid samples (~0.2 mL) were placed in 3D-printed liquid cells and sealed with Kapton tape. During data collection, samples were maintained at 80 K using an Oxford instruments cryostat. All XANES spectra were measured for at least two scans and averaged to improve the signal-to-noise ratio. Athena software with the IFEFFIT package were used to perform data averaging, energy calibration, and normalization of the spectra.

Abbreviations

[BMIM]	1-*n*-Butyl-3-methylimidazolium
δ-Cu$_{av}$	Ensemble average oxidation state of copper
CLS	Canadian Light Source
DMSO	Dimethylsulfoxide
HEPES	4-(2-Hydroxyethyl)-1-piperazineethanesulfonic acid
IL	Ionic liquid
MHB	Mueller Hinton Broth
MIC	Minimum inhibitory concentration
MBC	Minimum bactericidal concentration
NP	Nanoparticle
TAPIL	Tetraalkylphosphonium ionic liquid
SEM	Scanning electron microscopy
TEM	Transmission electron microscopy
XANES	X-ray absorption near edge spectroscopy

Author contributions

Conceptualization, AB & JFT; funding acquisition JFT & PK; investigation, AB, BRA, SD, RS, HZ, MS; methodology, AB, BRA,

SML PK, JFT; visualization, AB, SD, HZ; instrumental specialization, HZ, SML; project administration, JFT; supervision, JFT, PK; compiling experimental data, all authors; writing original draft, AB, SD, BRA; writing – review and editing, all authors. All authors have given approval to the final version of the manuscript.

Conflicts of interest

JF Trant is the CEO and President of Binary Star Research Services (BSRS). The company focuses on providing computational chemistry services to the private sector. BSRS has no financial interest in this published work, and no BSRS commercial concerns influenced the study or the conclusions of the work. ARB, SD, BRA, and JFT are listed co-inventors on a US provisional patent relating to these and related composites: "Antimicrobial Material Comprising a Tetraalkylphosphonium Ionic Liquid and Metal Nanoparticles" US provisional patent application #63/504,227 Filed May 25, 2023. This patent is the property of the University of Windsor.

References

1 C. G. Flegg, *An Introduction to Reading the Apocalypse*, St Vladimir's Seminary Press, Crestwood, NY, 1999.

2 K. C. Nicolaou and S. Rigol, *J. Antibiot.*, 2018, **71**, 153–184.

3 T. Pratchett and N. Gaiman, *Good Omens*, Gollancz, London, 1990.

4 C. Liu, Q. Zhou, Y. Li, L. V. Garner, S. P. Watkins, L. J. Carter, J. Smoot, A. C. Gregg, A. D. Daniels, S. Jervey and D. Albaiu, *ACS Cent. Sci.*, 2020, **6**, 315–331.

5 R. Sah, B. K. Padhi, A. Siddiq, A. Abdelaal, A. Reda, B. Ismail Lashin, A. Mohanty, N. Z. Alshahrani and A. J. Rodriguez-Morales, *Global Security: Health, Science And Policy*, 2022, **7**, 51–56.

6 J. Botelho, F. Grosso and L. Peixe, *Drug Resistance Updates*, 2019, **44**, 100640.

7 T. U. Berendonk, C. M. Manaia, C. Merlin, D. Fatta-Kassinos, E. Cytryn, F. Walsh, H. Bürgmann, H. Sørum, M. Norström, M.-N. Pons, N. Kreuzinger, P. Huovinen, S. Stefani, T. Schwartz, V. Kisand, F. Baquero and J. L. Martinez, *Nat. Rev. Microbiol.*, 2015, **13**, 310–317.

8 R. Irwin, *Medical Humanities*, 2022, **48**, 371–380.

9 J. H. Kwon and W. G. Powderly, *Science*, 2021, **373**, 471.

10 K. Sprigg and C. E. Pietrangeli, *Current Treatment Options in Infectious Diseases*, 2019, **11**, 42–57.

11 N. Bedrosian, E. Mitchell, E. Rohm, M. Rothe, C. Kelly, G. String and D. Lantagne, *Environ. Sci. Technol.*, 2020, **55**, 4162–4173.

12 G. Kampf, *J. Hosp. Infect.*, 2022, **127**, 101–110.

13 N. Kenters, E. G. Huijskens, S. C. de Wit, J. van Rosmalen and A. Voss, *Am. J. Infect. Control*, 2017, **45**, e69–e73.

14 N. Fuster-Valls, M. Hernández-Herrero, M. Marín-de-Mateo and J. J. Rodríguez-Jerez, *Food Control*, 2008, **19**, 308–314.

15 S. McEldowney and M. Fletcher, *Lett. Appl. Microbiol.*, 1988, **7**, 83–86.

16 H. Choi, P. Chatterjee, E. Lichtfouse, J. A. Martel, M. Hwang, C. Jinadatha and V. K. Sharma, *Environ. Chem. Lett.*, 2021, **19**, 1945–1951.

17 W. Han, Z. Wu, Y. Li and Y. Wang, *Chem. Eng. J.*, 2019, **358**, 1022–1037.

18 D. S. Cha and M. S. Chinnan, *Crit. Rev. Food Sci. Nutr.*, 2004, **44**, 223–237.

19 M. D. L. Balela and K. L. S. Amores, *Mater. Chem. Phys.*, 2019, **225**, 393–398.

20 N. Bharadishettar, K. U. Bhat and D. Bhat Panemangalore, *Metals*, 2021, **11**, 711.

21 C. Bergemann, S. Zaatreh, K. Wegner, K. Arndt, A. Podbielski, R. Bader, C. Prinz, U. Lembke and J. B. Nebe, *World Journal of Transplantation*, 2017, **7**, 193.

22 P. I. Hora, S. G. Pati, P. J. McNamara and W. A. Arnold, *Environ. Sci. Technol. Lett.*, 2020, **7**, 622–631.

23 N. Parveen, S. Chowdhury and S. Goel, *Environ. Sci. Pollut. Res. Int.*, 2022, **29**, 85742–85760.

24 R. E. Del Sesto, C. Corley, A. Robertson and J. S. Wilkes, *J. Organomet. Chem.*, 2005, **690**, 2536–2542.

25 K. J. Fraser and D. R. MacFarlane, *Aust. J. Chem.*, 2009, **62**, 309–321.

26 F. Postleb, D. Stefanik, H. Seifert and R. Giernoth, *Zeitschrift für Naturforschung B*, 2013, **68**, 1123–1128.

27 F. M. S. Costa, M. L. M. F. S. Saraiva and M. L. C. Passos, *J. Mol. Liq.*, 2022, **368**, 120750.

28 T. J. Cuthbert, T. D. Harrison, P. J. Ragogna and E. R. Gillies, *J. Mater. Chem. B*, 2016, **4**, 4872–4883.

29 P. Mester, A. K. Jehle, C. Leeb, R. Kalb, T. Grunert and P. Rossmanith, *RSC Adv.*, 2016, **6**, 32220–32227.

30 K. K. Thasneema, M. S. Thayyil, T. Rosalin, K. K. Elyas, T. Dipin, P. K. Sahu, N. S. Krishna Kumar, V. C. Saheer, M. Messali and T. B. Hadda, *J. Mol. Liq.*, 2020, **307**, 112960.

31 T. J. Cuthbert, B. Hisey, T. D. Harrison, J. F. Trant, E. R. Gillies and P. J. Ragogna, *Angew. Chem., Int. Ed.*, 2018, **57**, 12707–12710.

32 R. G. Carden, K. J. Sommers, C. L. Schrank, A. J. Leitgeb, J. A. Feliciano, W. M. Wuest and K. P. C. Minbiole, *ChemMedChem*, 2020, **15**, 1974–1984.

33 Y. Xue, H. Xiao and Y. Zhang, *Int. J. Mol. Sci.*, 2015, **16**, 3626–3655.

34 A. Banerjee, R. Theron and R. W. J. Scott, *ChemSusChem*, 2012, **5**, 109–116.

35 A. Banerjee and R. W. Scott, *Green Chem.*, 2015, **17**, 1597–1604.

36 A. Maclennan, A. Banerjee and R. W. Scott, *Catal. Today*, 2013, **207**, 170–179.

37 A. Banerjee, R. Theron and R. W. J. Scott, *Chem. Commun.*, 2013, **49**, 3227–3229.

38 A. Banerjee, R. Theron and R. W. Scott, *J. Mol. Catal. A: Chem.*, 2014, **393**, 105–111.

39 A. Banerjee, Y. Yao, M.-R. R. Durr, W. G. Barrett, Y. Hu and R. W. J. Scott, *Catal. Sci. Technol.*, 2018, **8**, 5207–5216.

40 A. Cieniecka-Rosłonkiewicz, J. Pernak, J. Kubis-Feder, A. Ramani, A. J. Robertson and K. R. Seddon, *Green Chem.*, 2005, **7**, 855–862.

41 N. V. Terekhova, L. S. Khailova, T. I. Rokitskaya, P. A. Nazarov, D. R. Islamov, K. S. Usachev, D. A. Tatarinov, V. F. Mironov, E. A. Kotova and Y. N. Antonenko, *ACS Omega*, 2021, **6**, 20676–20685.

42 V. V. Ermolaev, D. M. Arkhipova, V. A. Miluykov, A. P. Lyubina, S. K. Amerhanova, N. V. Kulik, A. D. Voloshina and V. P. Ananikov, *Int. J. Mol. Sci.*, 2021, **23**, 86.

43 I. Mukherjee, K. Manna, S. Ghosh and S. P. Moulik, *J. Chem. Eng. Data*, 2012, **57**, 1376–1386.

44 G. A. O'Toole, M. Wathier, M. E. Zegans, R. M. Shanks, R. Kowalski and M. W. Grinstaff, *Cornea*, 2012, **31**, 810.

45 S. Das, A. Paul, D. Bera, A. Dey, A. Roy, A. Dutta and D. Ganguly, *Mater. Today Commun.*, 2021, **28**, 102672.

46 L. O. Metelytsia, D. M. Hodyna, I. V. Semenyuta, V. V. Kovalishyn, S. P. Rogalsky, K. Y. Derevianko, V. S. Brovarets and I. V. Tetko, *Antibiotics*, 2022, **11**, 491.

47 J. N. Pendleton and B. F. Gilmore, *Int. J. Antimicrob. Agents*, 2015, **46**, 131–139.

48 M. Simões, A. R. Pereira, L. C. Simões, F. Cagide and F. Borges, *Drug Discovery Today*, 2021, **26**, 1340–1346.

49 S.-K. Ruokonen, C. Sanwald, M. Sundvik, S. Polnick, K. Vyavaharkar, F. Duša, A. J. Holding, A. W. T. King, I. Kilpeläinen, M. Lämmerhofer, P. Panula and S. K. Wiedmer, *Environ. Sci. Technol.*, 2016, **50**, 7116–7125.

50 M. V. Sanches, R. Freitas, M. Oliva, A. Cuccaro, G. Monni, A. Mezzetta, L. Guazzelli and C. Pretti, *Envrion. Sci. Pollut. Sci.*, 2023, **30**, 39288–39318.

51 F. Atefi, M. T. Garcia, R. D. Singer and P. J. Scammells, *Green Chem.*, 2009, **11**, 1595–1604.

52 K. L. Luska and A. Moores, *Green Chem.*, 2012, **14**, 1736–1742.

53 V. Ermolaev, D. Arkhipova, L. S. Nigmatullina, I. K. Rizvanov, V. Milyukov and O. Sinyashin, *Russ. Chem. Bull.*, 2013, **62**, 657–660.

54 A. P. Ingle, N. Duran and M. Rai, *Appl. Microbiol. Biotechnol.*, 2014, **98**, 1001–1009.

55 K. Kalwar and D. Shan, *Micro Nano Lett.*, 2018, **13**, 277–280.

56 D. Nakhaie, T. C. Williams, B. Velapatino, E. A. Bryce, M. K. Charles, E. Asselin and A. M. Clifford, *Adv. Mater. Interfaces*, 2022, **9**, 2201009.

57 European Committee for Standardization, Chemical disinfectants and antiseptics. Application of European standards for chemical disinfectants and antiseptics, (EN 14885), 2018.

58 European Committee for Standardization, Chemical disinfectants and antiseptics. Quantitative suspension test for the evaluation of fungicidal or yeasticidal activity in the

medical area—test method and requirements (phase 2, step 1), (EN 13624), 2013.

59 European Committee for Standardization, Chemicals used for the treatment of water intended for human consumption, ozone, (EN 1278), 2010.

60 European Committee for Standardization, Chemical disinfectants and antiseptics. Quantitative suspension test for the evaluation of bacterial activity in the medical area—test method and requirements (phase 2, step 1), (EN 13727:2012+A2:2015), 2015.

61 European Committee for Standardization, Chemical disinfectants and antiseptics—quantitative non-porous surface test for the evaluation of bactericidal and/or fungicidal activity of chemical disinfectants used in food, industrial, domestic and institutional areas—test method and requirements without mechanical action (phase 2, step 2), (EN 13697), 2015.

62 European Committee on Antimicrobial Susceptibility Testing, Breakpoint tables for interpretation of MICs and zone diameters, version 13.1, 2023.

63 N. Wald-Dickler, P. Holtom and B. Spellberg, *Clin. Infect. Dis.*, 2017, **66**, 1470–1474.

64 S. Fister, P. Mester, J. Sommer, A. K. Witte, R. Kalb, M. Wagner and P. Rossmanith, *Front. Microbiol.*, 2017, **8**, 1608.

65 P. Mester, M. Wagner and P. Rossmanith, *Ecotoxicol. Environ. Saf.*, 2015, **111**, 96–101.

66 N. Nikfarjam, M. Ghomi, T. Agarwal, M. Hassanpour, E. Sharifi, D. Khorsandi, M. Ali Khan, F. Rossi, A. Rossetti, E. Nazarzadeh Zare, N. Rabiee, D. Afshar, M. Vosough, T. Kumar Maiti, V. Mattoli, E. Lichtfouse, F. R. Tay and P. Makvandi, *Adv. Funct. Mater.*, 2021, **31**, 2104148.

67 J. Sommer, S. Fister, T. Gundolf, B. Bromberger, P.-J. Mester, A. K. Witte, R. Kalb and P. Rossmanith, *Int. J. Mol. Sci.*, 2018, **19**, 790.

68 J. Mock, M. Barbic, D. Smith, D. Schultz and S. Schultz, *J. Chem. Phys.*, 2002, **116**, 6755–6759.

69 B. Carlsson and G. Wettermark, *Z. Naturforsch. A*, 1976, **31**, 297–301.

70 A. N. Pestryakov, V. P. Petranovskii, A. Kryazhov, O. Ozhereliev, N. Pfänder and A. Knop-Gericke, *Chem. Phys. Lett.*, 2004, **385**, 173–176.

71 B. May, M. Lexow, N. Taccardi, H. P. Steinrück and F. Maier, *ChemistryOpen*, 2019, **8**, 15–22.

72 J. D. Vicente, D. C. Miguel, A. M. Gonçalves, D. M. Cabrita, J. M. Carretas, B. J. Vieira, J. C. Waerenborgh, D. Belo, A. P. Gonçalves and J. P. Leal, *Sustainable Chem.*, 2021, **2**, 63–73.

73 E. Ahmed and M. Ruck, *Dalton Trans.*, 2011, **40**, 9347–9357.

74 E. Ahmed, D. Koehler and M. Ruck, *Z. Anorg. Allg. Chem.*, 2009, **635**, 297–300.

75 C. Lamberti, S. Bordiga, F. Bonino, C. Prestipino, G. Berlier, L. Capello, F. D'Acapito, F. L. i Xamena and A. Zecchina, *Phys. Chem. Chem. Phys.*, 2003, **5**, 4502–4509.

76 A. Gaur, B. D. Shrivastava and S. K. Joshi, *J. Phys.: Conf. Ser.*, 2009, **190**, 012084.

77 Y. Zhou, F. Che, M. Liu, C. Zou, Z. Liang, P. De Luna, H. Yuan, J. Li, Z. Wang, H. Xie, H. Li, P. Chen, E. Bladt, R. Quintero-Bermudez, T.-K. Sham, S. Bals, J. Hofkens, D. Sinton, G. Chen and E. H. Sargent, *Nat. Chem.*, 2018, **10**(9), 974–980.

78 V. Mazalova and A. Soldatov, *J. Struct. Chem.*, 2008, **49**, 107–115.

79 S. Muzammil, M. Khurshid, I. Nawaz, M. H. Siddique, M. Zubair, M. A. Nisar, M. Imran and S. Hayat, *Biofouling*, 2020, **36**, 492–504.

80 M. A. Ansari, H. M. Khan, A. A. Khan, S. S. Cameotra, Q. Saquib and J. Musarrat, *J. Appl. Microbiol.*, 2014, **116**, 772–783.

81 N. Bruna, E. Galliani, P. Oyarzún, D. Bravo, F. Fuentes and J. M. Pérez-Donoso, *Biol. Res.*, 2022, **55**, 12.

82 Y. Wang and T. Asefa, *Langmuir*, 2010, **26**, 7469–7474.

83 J. Li, S. Xie, S. Ahmed, F. Wang, Y. Gu, C. Zhang, X. Chai, Y. Wu, J. Cai and G. Cheng, *Front. Pharmacol*, 2017, **8**, 364.

84 O. V. Zakharova, A. Y. Godymchuk, A. A. Gusev, S. I. Gulchenko, I. A. Vasyukova and D. V. Kuznetsov, *BioMed Res. Int.*, 2015, **2015**, 412530.

85 C. A. P. Bastos, N. Faria, J. Wills, P. Malmberg, N. Scheers, P. Rees and J. J. Powell, *NanoImpact*, 2020, **17**, 100192.

86 P. Lambert, *J. R. Soc. Med.*, 2002, **95**, 22.

87 K. Konaté, J. F. Mavoungou, A. N. Lepengué, R. R. Aworet-Samseny, A. Hilou, A. Souza, M. H. Dicko and B. M'Batchi, *Ann. Clin. Microbiol. Antimicrob.*, 2012, **11**, 1–12.

88 M. L. Ermini and V. Voliani, *ACS Nano*, 2021, **15**, 6008–6029.

89 A. N. Pham, G. Xing, C. J. Miller and T. D. Waite, *J. Catal.*, 2013, **301**, 54–64.

90 C.-H. Hu and M.-S. Xia, *Appl. Clay Sci.*, 2006, **31**, 180–184.

91 Z. Zheng, Q. Xu, J. Guo, J. Qin, H. Mao, B. Wang and F. Yan, *ACS Appl. Mater. Interfaces*, 2016, **8**, 12684–12692.

92 J. Thiel, L. Pakstis, S. Buzby, M. Raffi, C. Ni, D. e. J. Pochan and S. I. Shah, *Small*, 2007, **3**, 799–803.

93 C. Zhou, F. Wang, H. Chen, M. Li, F. Qiao, Z. Liu, Y. Hou, C. Wu, Y. Fan and L. Liu, *ACS Appl. Mater. Interfaces*, 2016, **8**, 4242–4249.

94 A. Borkowski, Ł. Ławniczak, T. Cłapa, D. Narożna, M. Selwet, D. Pęziak, B. Markiewicz and Ł. Chrzanowski, *Ecotoxicol. Environ. Saf.*, 2016, **130**, 54–64.

95 C. Peng, Y. Liu, L. Shui, Z. Zhao, X. Mao and Z. Liu, *Life*, 2022, **12**, 1581.

96 N. Ghasedi, S. Ahmadi, S. Ketabi and A. Almasirad, *J. Recept. Signal Transduction*, 2022, **42**, 418–428.

97 We wish to emphasize that this comparison is for illustrative purposes only; these reported composites need additional study before they could be used, and detailed toxicology and studies on their persistence and environmental impact needs to be carried out before they could be considered for any particular application.